

## Supporting Information

### Direct Integration of Polycrystalline Graphene on Silicon as Photodetector via Plasma-Assisted Chemical Vapor Deposition

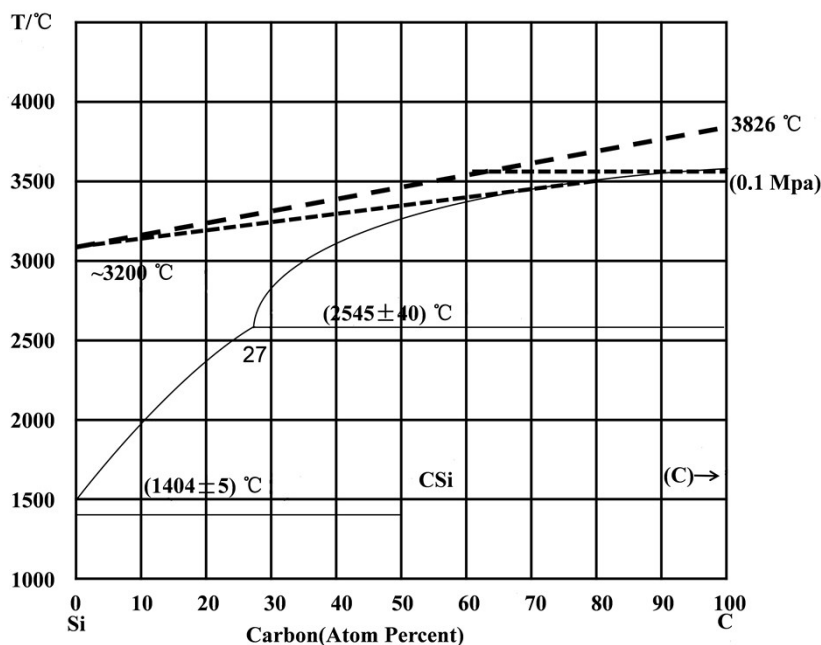
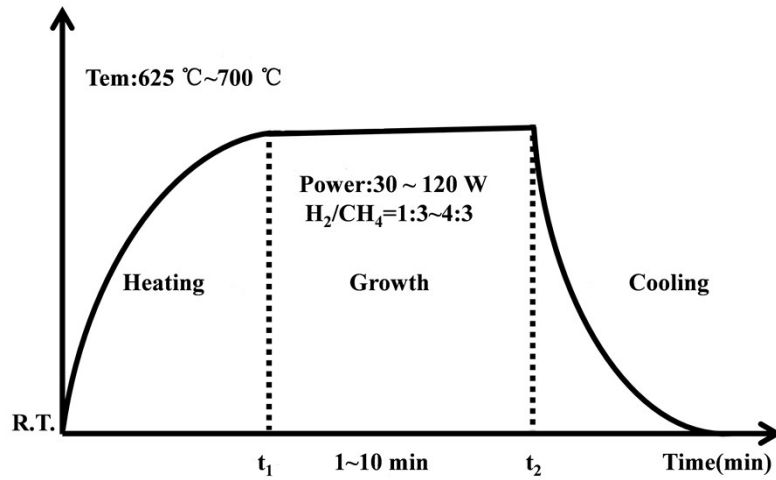


Fig. S1 Phase diagrams of the selected binary systems: Si-C.<sup>[1]</sup>

### Experimental details



Fig. S2 The photograph of the PACVD system used for growing graphene directly on Si substrate.



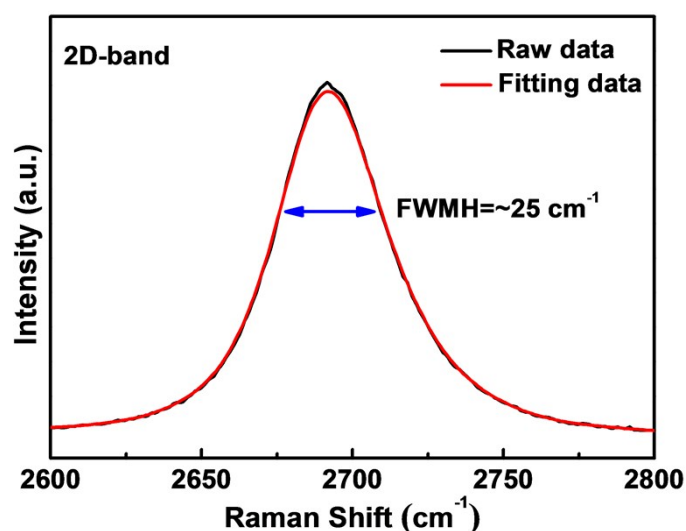
**Fig. S3** Schematic illustrating the preparation of graphene films by PACVD.

***Graphene Preparation:***

The Si substrates (110, 525  $\mu\text{m}$  thick, n-type) were cut into  $1 \times 1 \text{ cm}^2$  pieces and chemically cleaned (HF buffer etching solution) to remove thin the native oxide silicon on the surface before the graphene growth. Then, placed at the center of the horizontal quartz tube. The synthesis was carried out in a horizontal tube furnace inside a quartz processing tube (60 mm inner diameter). Prior to heating, the quartz tube was evacuated to approximately  $10^{-5}$  mbar. And then introduced the continuous flow of 10 standard cubic cm per min (sccm) argon (Ar, 99.9999% purity) and 1 sccm hydrogen ( $\text{H}_2$ , 99.9999% purity) until 0.14 mbar. After heating to the desired temperature (varied from 625  $^\circ\text{C}$  to 700  $^\circ\text{C}$ ),  $\text{H}_2$  to methane ( $\text{CH}_4$ ) gas ratios (varied from 1:3 to 4: 3 sccm) were introduced to deposit the graphene film for different time durations (from 1 min to 10 min) under varying the plasma power (changed from 120 W to 30 W). After deposition, the plasma power shut down and then the  $\text{CH}_4$  gas was turned off. Subsequently, the furnace was cooled to room temperature. The process is summarized in **Fig. S3**.

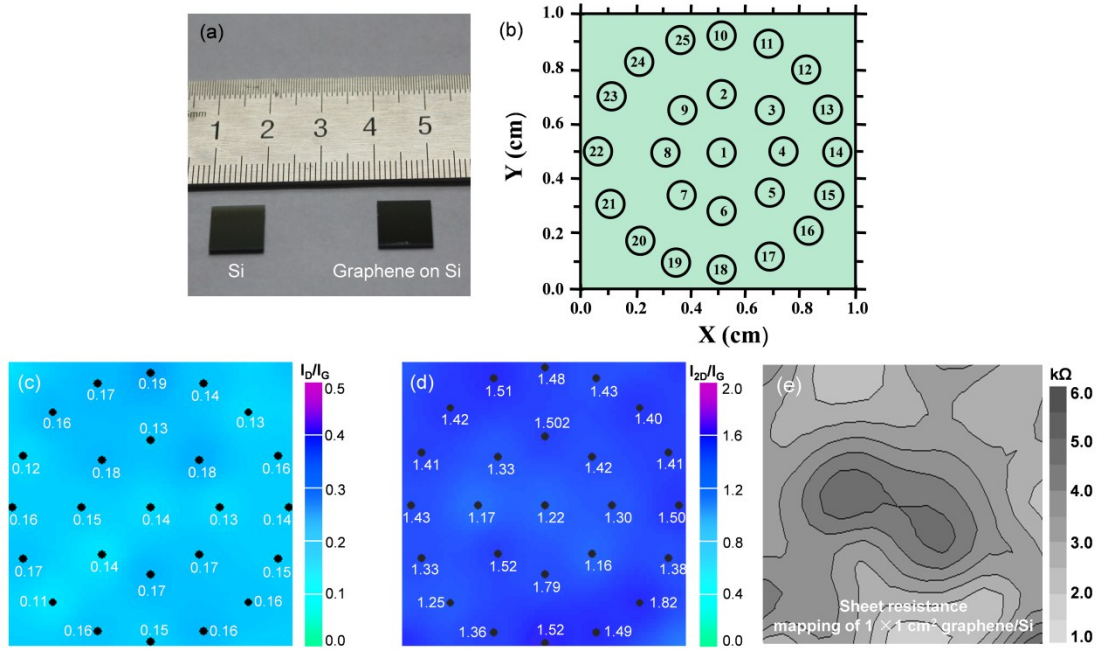
### **Graphene Transfer:**

Graphene films were transferred from the Si substrate onto a highly-doped p-Si wafer with a 300 nm thermal oxide by a PMMA-assisted wet-transfer method in order to evaluate the electrical transport properties. A thin layer of polymethyl methacrylate (Micro Chem 950 PMMA C, 3% in chlorobenzene) was spin-coated onto the substrate to protect the graphene film and to act as a support which was then cured at 100 °C for 20 min. Afterwards, the Si substrate was etched away by a mixture of potassium dichromate ( $K_2Cr_2O_7$ ) :  $H_2O$  : hydrofluoric acid (HF, 42%) = 11g : 250 ml : 500 ml allowing the PMMA/graphene layer to float on top of the solution. After placing the layer on a filter paper, it was washed with deionized water. The PMMA/graphene layer was subsequently transferred to another substrate (i.e., quartz slides,  $SiO_2$  and TEM grid) followed by annealing at 150 °C for 100 min to improve adhesion. The PMMA was then dissolved gradually with acetone and deionized water. Finally, the graphene sample was washed with isopropanol and then annealed under flowing Ar (10 sccm) and  $H_2$  (100 sccm) for 5 h at 300 °C to remove the residual PMMA.



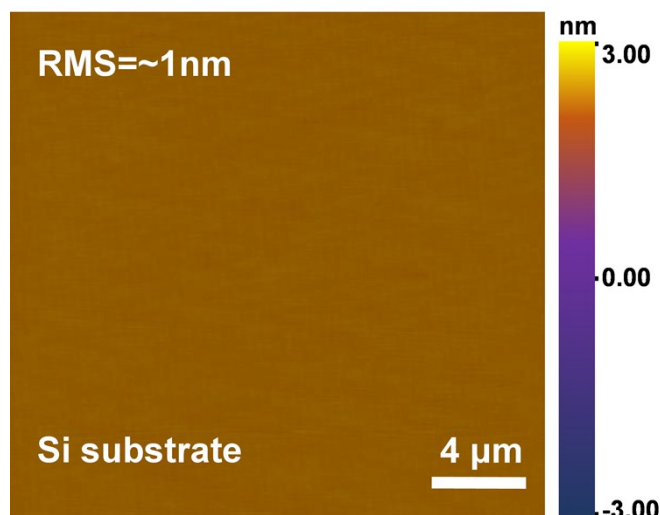
**Fig. S4** The FWHM and the Lorentzian fitting of 2D band.

Fig. S4 (ESI) shows the symmetric 2D peak with a FWHM of  $\sim 25 cm^{-1}$  can be well fitted by a single Lorentzian curve providing evidence of monolayered graphene.<sup>[2]</sup>



**Fig. S5** (a) Photographs of the Si substrate and graphene covered Si substrate. (b) Twenty five points are selected from an area of  $1 \times 1 \text{ cm}^2$  for Raman measurement. (c) and (d)  $I_D/I_G$  peak and  $I_{2D}/I_G$  peak ratio derived from Raman mapping over an area of  $1 \times 1 \text{ cm}^2$  on the monolayer graphene. (e) A contour mapping for sheet resistance of as-growth graphene.

To evaluate the large-scale uniformity, **Fig. S5(a)** provides the optical images of the graphene on Si substrate with dimensions of  $1 \times 1 \text{ cm}^2$ . The contrast between the bare area and major area covered by graphene on Si substrate. By increasing the diameter of the quartz tube to accommodate the Si substrates, graphene films with the wafer scale are expected and the associated work is in progress. To determine the uniformity of the graphene, 25 points uniformly distributed over the area of  $1 \times 1 \text{ cm}^2$  are analyzed by Raman scattering, as shown in **Fig. S5(b)**. Using the software *Wafer Viewer*, the  $I_D/I_G$  peak ratio and  $I_{2D}/I_G$  peak ratio mapping are obtained and plotted in **Fig. S5(c)** and **Fig. S5(d)**. The  $I_D/I_G$  and the  $I_{2D}/I_G$  ratios calculated from the 25 points are in the range of 0.12~0.19 and 1.16~1.82, respectively, suggesting the formation of monolayer graphene with good uniformity over a area of  $1 \times 1 \text{ cm}^2$ . The sheet resistance contour map analysis of  $1 \times 1 \text{ cm}^2$  as-growth graphene is shown in **Fig. S5(e)**. The mean value of  $R_{sq}$  is 1~6  $\text{k}\Omega/\text{sq}$ .



**Fig. S6** The surface morphology and roughness analysis of annealed Si substrate.

In order to accurately assess the roughness of graphene on Si substrate and to eliminate the impact of the substrate. The utilized Si was firstly annealed at 700 °C in Ar and H<sub>2</sub> (1:4 sccm gas flow rate) for 10 min under plasma (power: 30 W). As measured from the annealed Si sample, the surface roughness is equal to ~1 nm over a scanned area of 20 × 20 μm<sup>2</sup>, as shown in **Fig. S6**.

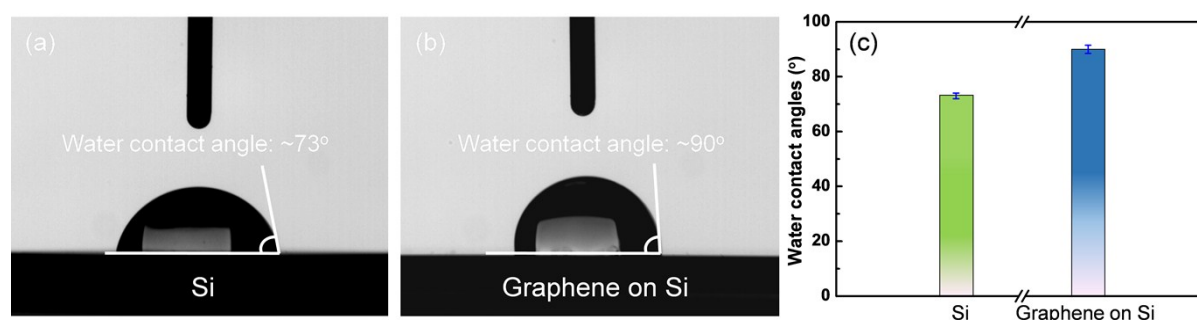


**Fig. S7** The water contact angle of the (a) Si substrate and (b) as-synthesized graphene on Si substrate. (c) Histogram of the water contact angle distribution for Si substrate and as-synthesized graphene on Si substrate, respectively.

In order to perform respective wetting angle measurements to study the evolution wettability of Si substrate. The contact angle was measured using a JCY-1 digital goniometer equipped with a microsyringe. A 1 mL water droplet was generated using the goniometer,

based on four time-controlled volume steps of 0.25 mL close to the sample surface. The sessile droplet was formed by fixing the needle and approaching the substrate parallel to the needle direction with a very gentle feed rate of a few micrometers per minute. All the tests were performed under ambient conditions. For the Si substrate (**Fig. S7(a)**), we find that the contact angle of the Si substrate (without graphene film coating) is  $\sim 73^\circ$ .<sup>[3]</sup> When graphene was deposited on the Si substrate, we observed complete hydrophobic, i.e., contact angle is  $\sim 90^\circ$ ,<sup>[4]</sup> as shown in **Fig. S7(b)**. **Fig. S7(c)** shows histogram of the water contact angle distribution for Si substrate and as-synthesized graphene on Si substrate, respectively.

### ***Device fabrication and electrical transport measurement***

The electronic transport measurements of the as-synthesized graphene films are evaluated using the back-gated graphene field effect transistors (GFETs) to reveal the carrier mobility. The as-synthesized graphene films were transferred to highly doped p-Si substrate with a 300 nm thick thermal oxide, followed by deposition of source and drain electrodes with Au/Ti (50/10 nm) by electron beam evaporation. Afterwards, another photolithographic step employing inductively coupled plasma (ICP) was used to pattern the doped graphene to form a field-effect transistor with a channel length of 8  $\mu\text{m}$  and width of 2  $\mu\text{m}$ . To improve the contact of the back-gated GFETs device, annealing was performed in Ar (200 sccm) and  $\text{H}_2$  (10 sccm) at 300  $^\circ\text{C}$  for 6 h in a tube furnace. The back-gated GFETs were characterized under ambient conditions using the Agilent (B1500A) semiconductor parameter analyzer. The mobility was extracted using the following equation:<sup>[5]</sup>

$$\mu_{FET} = \frac{dI_{DS}}{dV_G} \cdot \frac{L}{W \cdot C_{ox} \cdot V_{DS}}$$

where L and W are the channel length and width,  $C_{ox}$  is the gate oxide capacitance (11  $\text{nF} \cdot \text{cm}^{-2}$ ),  $V_{DS}$  is the source drain voltage,  $I_{DS}$  is the source drain current, and  $V_G$  is the gate voltage. The linear regime of the transfer characteristics was used to obtain  $dI_{DS}/dV_G$ .

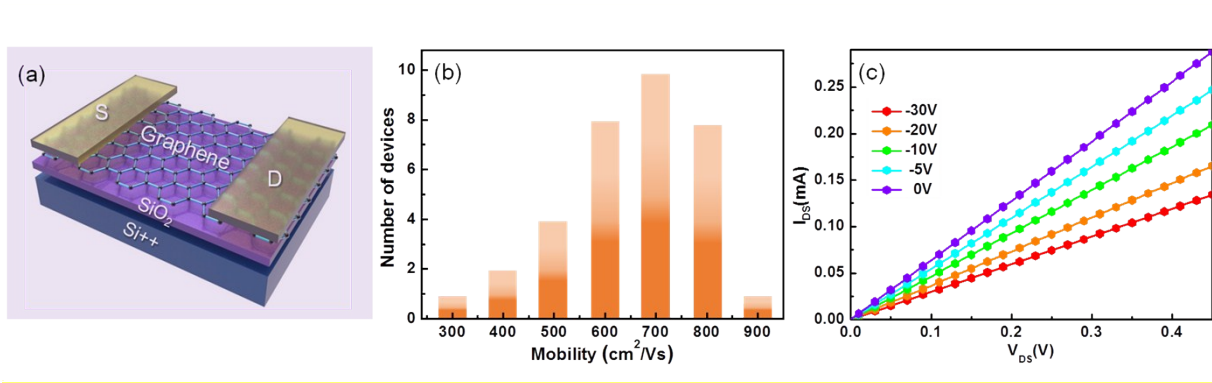


**Fig. S8** (a) Schematic diagram of the back-gated GFET device. (b) Histogram of the field effect mobility distribution for total 34 devices. (c) Output ( $I_{DS}$ - $V_{DS}$ ) characteristics of the GFET at different  $V_G$ .

**Fig. S8(a)** shows the schematic diagram of the fabricated GFETs, and the corresponding SEM image is shown in the inset. Histogram of the field effect mobility distribution for total 34 devices demonstrates that the as-synthesized graphene exhibits carrier mobilities in the range of  $600\sim 700\text{ cm}^2\text{V}^{-1}\text{s}^{-1}$  for holes and  $500\sim 600\text{ cm}^2\text{V}^{-1}\text{s}^{-1}$  for electrons, as shown in **Fig. S8(b)**, which are comparable to the carrier mobilities reported for graphene synthesized on metal by PECVD.<sup>[6-7]</sup> The output characteristics of the as-synthesized graphene is shown in **Fig. S8(c)**. The linear  $I_{DS}$ - $V_{DS}$  behavior indicates a good ohmic contact between the Ti/Au contact and pristine graphene channels. In addition,  $I_{DS}$  increases with decreasing  $V_G$ , suggesting a p-type behavior in the graphene structures.

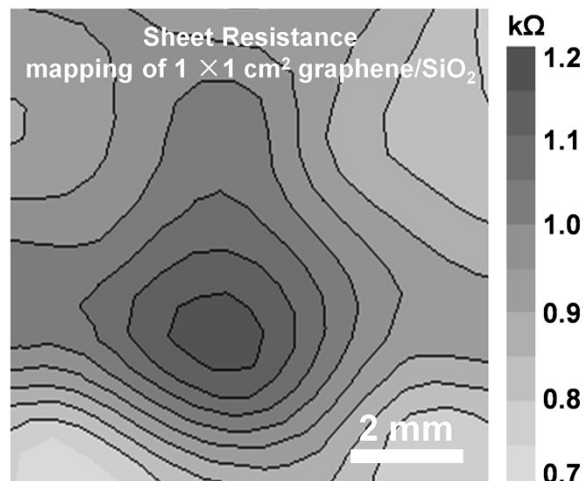


**Fig. S9** A contour mapping for sheet resistance of as-growth graphene.

After graphene preparation, the films transferred onto the SiO<sub>2</sub>/Si substrate by a PMMA-assisted wet-transfer method. The four-probe resistance measurement was carried out to determine the resistivity in Ohm per square. The sheet resistance contour map analysis of 1 × 1 cm<sup>2</sup> is shown in **Fig. S9**. The mean value of Rsq is in the range of 0.7~1 kΩ/sq.

### ***Photoelectrical measurements of the graphene/Si Schottky junctions***

In order to evaluate the photoelectrical properties of the as-synthesized graphene film, photodectors were directly fabricated on Si substrate bypass the transfer process. Deposition of electrodes with Ag (200 nm) by electron beam evaporation. The photodectors were characterized under ambient conditions using the Agilent (B1500A) semiconductor parameter analyzer and Keithley 4200 semiconductor characterization system. To quantify the performance, two key metrics including the responsivity ( $R$ ) and detectivity ( $D^*$ ) reflecting the photodetector sensitivity to incident light were calculated by the following equations:<sup>[8-9]</sup>

$$R = \frac{I_p}{P_{opt}} = \eta \left( \frac{q\lambda}{hc} \right) G$$

$$D^* = \frac{R}{(2qJ_{dark} / A)^{1/2}}$$

where  $I_p$ ,  $P_{opt}$ ,  $\eta$ ,  $h$ ,  $c$ ,  $\lambda$ ,  $A$ ,  $q$ ,  $I_{dark}$  and  $G$  are the photocurrent, incident light power, quantum efficiency, Planck's constant, speed of light, light wavelength, active area, elementary charge, dark current, and photoconductive gain, respectively.

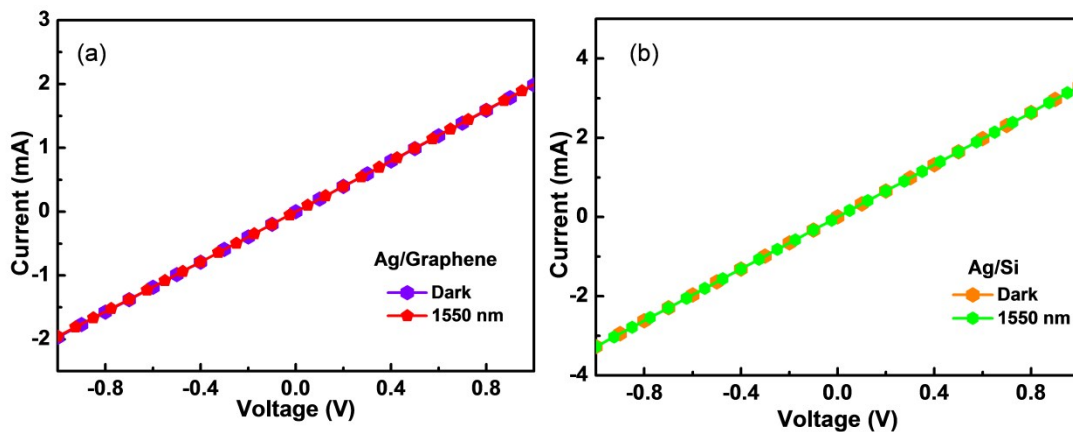


**Fig. S10** (a) I-V characteristics of the Ag/graphene measured at room temperature with and without 1550 nm irradiation. (b) I-V characteristics of the Ag/Si contact measured at room temperature with and without 1550 nm irradiation.

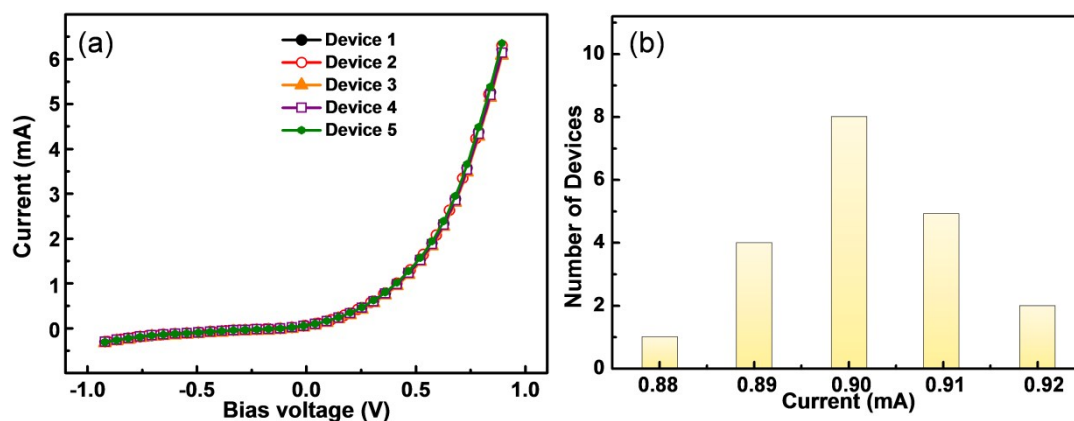


**Fig. 11** (a)  $I_{ds}$ - $V_{ds}$  characteristics of 5 representative photodetectors measured under light illumination with wavelengths of 1550 nm, the light intensity of the light sources is fixed at  $10 \text{ mW/cm}^2$ . (b) The distributional histogram of the photocurrent collected at  $V_{ds} = 0.5 \text{ V}$  for 20 devices.

For the reproducibility issue, more than 20 graphene/Si Schottky junctions have been tested, as shown in Figure R-v. From  $I_{ds}$ - $V_{ds}$  curves collected from 5 representative devices as displayed in **Fig. 11 (a)**, it is observed that the rectification behaviors are obtained in all selected photodetectors constructed on the graphene/Si Schottky junction, and the rectification ratios are quite similar. For the photocurrents collected at  $V_{ds} = 0.5 \text{ V}$  from 20 individual photodetectors, the photocurrent histogram reveals that the majority of photocurrent is in the range from 0.88 to 0.92 mA with an average value of 0.9 mA, as provided in **Fig. 11 (b)**, indicating the photodetector devices constructed on the graphene/Si Schottky junction exhibit excellent reproducibility.

## Supplementary References

[1] R. W. Olesinski and G. J. Abbaschian, *Bulletin of alloy phase diagrams*, 1984, **5**, 486-489.

- [2] J. Park, W. C. Mitchel, L. Grazulis, H. E. Smith, K. G. Eyink, J. J. Boeckl and J. Hoelscher, *Adv. Mater.*, 2010, **22**, 4140-4145.
- [3] C. W. Extrand and Y. Kumaga, *J. Colloid. Interface. Sci.*, 1997, **191**, 378-383.
- [4] G. Hong, Y. Han, T. M. Schutzius, Y. Wang, Y. Pan, M. Hu, J. S. Jie, C. S. Sharma, U. Muller and D. Poulikakos, *Nano Lett.*, 2016, **16**,4447-4453.
- [5] G. Liu, W. Stillman, S. Rumyantsev, Q. Shao, M. Shur and A. A. Balandin, *Appl. Phys. Lett.*, 2009, **95**, 033103.
- [6] D. C. Wei, Y. H. Lu, C. Han, T. C. Niu, W. Chen and A. T. S. Wee, *Angew. Chem. Int. Ed*, 2013, **52**, 14121.
- [7] K. J. Peng, C. L. Wu, Y. H. Lin, Y. J. Liu, D. P. Tsai, Y. H. Paic and G. R. Lin, *J. Mater. Chem. C*, 2013, **1**, 3862-3870.
- [8]. L. H. Zeng, M. Z. Wang, H. Hu, B. Nie, Y. Q. Yu, C. Y. Wu, L. Wang, J. G. Hu, C. Xie, F. X. Liang and L. B. Luo, *ACS Appl. Mater. Interfaces.*, 2013, **5**, 9362-9366.
- [9] X. Liu, L. L. Gu, Q. P. Zhang, J. Y. Wu, Y. Z. Long and Z. Y. Fan, *Nat. Commun.*, 2014, **5**, 4007.